

# Image Denoising Using Transformed L1 (TL1) Regularization via ADMM

Nabiha Choudhury<sup>1</sup>, Jianqing Jia<sup>2</sup>, Yifei Lou<sup>1,2</sup>

<sup>1</sup>Department of Mathematics, University of North Carolina at Chapel Hill, Chapel Hill, NC, USA

<sup>2</sup>School of Data Science and Society, University of North Carolina at Chapel Hill, Chapel Hill, NC, USA

Emails: chnabi@unc.edu, jqjia@unc.edu, yflou@unc.edu

**Abstract**—Total variation (TV) regularization is a classical tool for image denoising, but its convex  $\ell_1$  formulation often leads to staircase artifacts and loss of contrast. To address these issues, we introduce the Transformed  $\ell_1$  (TL1) regularizer applied to image gradients. In particular, we develop a TL1-regularized denoising model and solve it using the Alternating Direction Method of Multipliers (ADMM), featuring a closed-form TL1 proximal operator and an FFT-based image update under periodic boundary conditions. Experimental results demonstrate that our approach achieves superior denoising performance, effectively suppressing noise while preserving edges and enhancing image contrast.

**Index Terms**—Image denoising, Transformed  $\ell_1$ , Alternating Direction Method of Multipliers, Proximal operator

## I. INTRODUCTION

Image denoising is a fundamental task in image processing, aiming to recover a clean image from its noisy observations. Variational methods with sparsity-promoting priors have shown great success in removing noise while preserving structural details. Among these, gradient-based techniques have gained prominence by exploiting the fact that natural images typically have sparse gradients, considering that most regions are smooth, while edges appear as sharp discontinuities. By applying regularization directly to image gradients, these methods can separate noise from true image features, achieving strong noise suppression with superior edge preservation.

Total Variation (TV) [1] is a classical regularization method that applies the convex  $\ell_1$  norm to promote gradient sparsity. However, because  $\ell_1$  is a convex relaxation to the  $\ell_0$  norm, which directly counts nonzero elements, TV often produces staircase artifacts and causes loss of image contrast. Since the  $\ell_0$  norm is discontinuous and difficult to optimize, non-convex regularizers that strike a balance between these two extremes have attracted considerable attention. For example, Lou et al. [2] proposed the  $\ell_1$ – $\ell_2$  regularization on the gradient, leading to a weighted difference of the anisotropic and isotropic TV formulation. In addition, Minimax Concave Penalty (MCP) and the  $\ell_1$ – $\ell_2$  regularization were investigated in [3] and [4], respectively.

In this paper, we advocate the use of the Transformed  $\ell_1$  (TL1) regularizer on the gradient for image denoising. TL1 [5] has emerged as an attractive non-convex penalty that provides a smooth interpolation between  $\ell_0$  and  $\ell_1$  norms. By adjusting a single parameter, TL1 can transition from promoting aggressive sparsity (similar to  $\ell_0$ ) to encouraging moderate sparsity with convex-like behavior (similar to  $\ell_1$ ).

This flexibility offers improved sparsity and edge preservation compared to TV, making it particularly well-suited for image reconstruction tasks. We solve the proposed model using the Alternating Direction Method of Multipliers (ADMM) [6], which efficiently decouples the non-smooth penalty from the data fidelity term, leading to high-quality reconstructions that leverage both the adaptive sparsity of TL1 and the edge-preserving properties of gradient-based regularization.

## II. THE PROPOSED APPROACH

Let  $U \in \mathbb{R}^{N \times M}$  denote a 2D image of size  $N \times M$ , and let  $\mathbf{u} = \text{vec}(U) \in \mathbb{R}^{NM}$  be its vectorized representation obtained by stacking all pixels following the linear index. The spatial derivatives of  $U$  along the horizontal and vertical directions are defined by

$$(D_x U)_{i,j} = U_{i,j+1} - U_{i,j}, \quad (D_y U)_{i,j} = U_{i+1,j} - U_{i,j},$$

respectively, under periodic boundary conditions. We define the discrete difference operators  $D_x$  and  $D_y$  such that  $D_x U$  and  $D_y U$  approximate the partial derivatives of  $U$  with respect to the  $x$ - and  $y$ -coordinates. When acting on the vectorized image  $\mathbf{u}$ , the same notations  $D_x$  and  $D_y$  refer to their matrix representations satisfying  $D_x \mathbf{u} = \text{vec}(D_x U)$  and  $D_y \mathbf{u} = \text{vec}(D_y U)$ . Consequently, the discrete gradient operator  $\nabla : \mathbb{R}^{NM} \rightarrow \mathbb{R}^{2NM}$  is defined as

$$\nabla \mathbf{u} = (D_x \mathbf{u}, D_y \mathbf{u}). \quad (1)$$

The TL1 function [5] for a vector  $\mathbf{x} \in \mathbb{R}^n$  is defined as

$$\text{TL1}_a(\mathbf{x}) = \sum_{i=1}^n \frac{(a+1)|x_i|}{a+|x_i|}, \quad (2)$$

where  $a > 0$  is a shape parameter controlling the degree of nonconvexity. Smaller  $a$  values yield a more nonconvex penalty that more aggressively enforces sparsity, while larger  $a$  values make the function smoother and asymptotically approach the convex  $\ell_1$  norm.

We propose applying the TL1 penalty to the image gradients, i.e.,

$$J(\mathbf{u}) = \sum_{i,j} [\text{TL1}_a((D_x \mathbf{u})_{i,j}) + \text{TL1}_a((D_y \mathbf{u})_{i,j})], \quad (3)$$

which is referred to as TL1 regularization, with a slight abuse of terminology. This regularization promotes sparsity in the

image gradients, encouraging piecewise-constant reconstructions and preserving sharp edges.

We incorporate the TL1 regularization (3) into the standard denoising formulation

$$\min_{\mathbf{u} \in \mathbb{R}^{NM}} J(\mathbf{u}) + \frac{\mu}{2} \|\mathbf{u} - \mathbf{f}\|_2^2, \quad (4)$$

where  $\mathbf{f}$  represents the noisy image in vectorized form and  $\mu > 0$  controls the balance between data fidelity and regularization.

To solve the proposed denoising problem (4), we employ ADMM to decouple the data fidelity and nonconvex regularization terms, allowing each subproblem to be handled efficiently. To facilitate the ADMM optimization, we introduce auxiliary variables

$$\mathbf{d}_x = D_x \mathbf{u}, \quad \mathbf{d}_y = D_y \mathbf{u}, \quad (5)$$

reformulating (4) as a constrained problem

$$\begin{aligned} \min_{\mathbf{u}, \mathbf{d}_x, \mathbf{d}_y} \quad & \sum_{i,j} \left[ \text{TL1}_a((\mathbf{d}_x)_{i,j}) + \text{TL1}_a((\mathbf{d}_y)_{i,j}) \right] + \frac{\mu}{2} \|\mathbf{u} - \mathbf{f}\|_2^2 \\ \text{s.t.} \quad & \mathbf{d}_x = D_x \mathbf{u}, \quad \mathbf{d}_y = D_y \mathbf{u}. \end{aligned} \quad (6)$$

Let  $\mathbf{b}_x$  and  $\mathbf{b}_y$  denote the dual variables associated with the constraints  $\mathbf{d}_x = D_x \mathbf{u}$  and  $\mathbf{d}_y = D_y \mathbf{u}$ , respectively. The augmented Lagrangian corresponding to (6) is written as

$$\begin{aligned} & \mathcal{L}(\mathbf{u}, \mathbf{d}_x, \mathbf{d}_y; \mathbf{b}_x, \mathbf{b}_y) \\ &= \sum_{i,j} [\text{TL1}_a((\mathbf{d}_x)_{i,j}) + \text{TL1}_a((\mathbf{d}_y)_{i,j})] + \frac{\mu}{2} \|\mathbf{u} - \mathbf{f}\|_2^2 \\ & \quad + \frac{\lambda}{2} (\|\mathbf{d}_x - D_x \mathbf{u} - \mathbf{b}_x\|_2^2 + \|\mathbf{d}_y - D_y \mathbf{u} - \mathbf{b}_y\|_2^2), \end{aligned} \quad (7)$$

where  $\lambda > 0$  is the penalty parameter. The ADMM iterations are summarized as follows:

$$\begin{cases} \mathbf{u}^{k+1} := \arg \min_{\mathbf{u}} \mathcal{L}(\mathbf{u}, \mathbf{d}_x^k, \mathbf{d}_y^k; \mathbf{b}_x^k, \mathbf{b}_y^k), \\ \mathbf{d}_x^{k+1} := \arg \min_{\mathbf{d}_x} \mathcal{L}(\mathbf{u}^{k+1}, \mathbf{d}_x, \mathbf{d}_y^k; \mathbf{b}_x^k, \mathbf{b}_y^k), \\ \mathbf{d}_y^{k+1} := \arg \min_{\mathbf{d}_y} \mathcal{L}(\mathbf{u}^{k+1}, \mathbf{d}_x^{k+1}, \mathbf{d}_y; \mathbf{b}_x^k, \mathbf{b}_y^k), \\ \mathbf{b}_x^{k+1} := \mathbf{b}_x^k + (D_x \mathbf{u}^{k+1} - \mathbf{d}_x^{k+1}), \\ \mathbf{b}_y^{k+1} := \mathbf{b}_y^k + (D_y \mathbf{u}^{k+1} - \mathbf{d}_y^{k+1}). \end{cases} \quad (8)$$

We elaborate on the details of solving these subproblems in (8) in the subsequent subsections.

### A. Image Variable Update

The image variable  $\mathbf{u}$  is updated while keeping  $(\mathbf{d}_x, \mathbf{d}_y)$  and  $(\mathbf{b}_x, \mathbf{b}_y)$  fixed. By setting the derivative of (7) with respect to  $\mathbf{u}$  to zero, we obtain the following linear system:

$$\begin{aligned} & (\mu I + \lambda D_x^\top D_x + \lambda D_y^\top D_y) \mathbf{u}^{k+1} \\ &= \mu \mathbf{f} + \lambda D_x^\top (\mathbf{d}_x^k - \mathbf{b}_x^k) + \lambda D_y^\top (\mathbf{d}_y^k - \mathbf{b}_y^k). \end{aligned} \quad (9)$$

Under periodic boundary conditions, both  $D_x$  and  $D_y$  are circulant matrices, and thus  $D_x^\top D_x + D_y^\top D_y$  corresponds to a discrete Laplacian operator that can be diagonalized by the two-dimensional (2D) Fourier transform. This property allows

$\mathbf{u}^{k+1}$  to be updated efficiently using FFT. Define the Laplacian kernel

$$\begin{aligned} K[0,0] &= 4, \quad K[0,1] = -1, \quad K[1,0] = -1, \\ K[N-1,0] &= -1, \quad K[0,M-1] = -1, \end{aligned} \quad (10)$$

with all other entries being zero. The corresponding closed-form update in the frequency domain is given by

$$\mathbf{u}^{k+1} = \mathcal{F}^{-1} \left( \frac{\mathcal{F}[\mathbf{r}^k]}{\mu + \lambda \mathcal{F}[K]} \right), \quad (11)$$

where  $\mathbf{r}^k = \mu \mathbf{f} + \lambda D_x^\top (\mathbf{d}_x^k - \mathbf{b}_x^k) + \lambda D_y^\top (\mathbf{d}_y^k - \mathbf{b}_y^k)$ ,  $\mathcal{F}$  denotes the 2-D discrete Fourier transform, and the division is performed element-wise in the frequency domain. This FFT-based implementation reduces the computational complexity of solving (9) from  $O((NM)^3)$  to  $O(NM \log(NM))$ .

### B. Proximal Operator

Given a proper function  $f : \mathbb{R} \rightarrow \mathbb{R}$ , the proximal operator [7] of  $f$  with parameter  $\beta > 0$  at  $x$  is defined as

$$\text{prox}_{\beta f}(x) = \arg \min_{v \in \mathbb{R}} \left\{ f(v) + \frac{1}{2\beta} (v - x)^2 \right\}. \quad (12)$$

For separable regularizers (those that can be written as sums over components), the proximal operator can be computed elementwise on vectors.

In the ADMM iterations (8), the TL1 regularizer is involved in both  $\mathbf{d}_x$ - and  $\mathbf{d}_y$ -subproblems. Since TL1 is separable over entries, the updates of  $\mathbf{d}_x$  and  $\mathbf{d}_y$  can be written as

$$\mathbf{d}_x^{k+1} = \text{prox}_{\frac{1}{\lambda} \text{TL1}_a}(\mathbf{z}_x^k), \quad \mathbf{d}_y^{k+1} = \text{prox}_{\frac{1}{\lambda} \text{TL1}_a}(\mathbf{z}_y^k),$$

where  $\mathbf{z}_x^k := D_x \mathbf{u}^{k+1} + \mathbf{b}_x^k$ ,  $\mathbf{z}_y^k := D_y \mathbf{u}^{k+1} + \mathbf{b}_y^k$ , and the proximal operator is applied componentwise. Specifically, for a vector  $\mathbf{z}$  with entries  $z_\ell$ ,

$$\text{prox}_{\frac{1}{\lambda} \text{TL1}_a}(\mathbf{z}) := (\text{prox}_{\frac{1}{\lambda} \text{TL1}_a}(z_\ell))_\ell,$$

and the scalar TL1 proximal mapping is defined by

$$\text{prox}_{\frac{1}{\lambda} \text{TL1}_a}(x) = \arg \min_{v \in \mathbb{R}} \left\{ \frac{(a+1)|v|}{a+|v|} + \frac{\lambda}{2} (v - x)^2 \right\}, \quad (13)$$

which admits a closed-form solution detailed in [8]. In implementation, we apply the closed-form TL1 proximal operator to each entry of  $\mathbf{z}_x^k$  and  $\mathbf{z}_y^k$  to obtain  $\mathbf{d}_x^{k+1}$  and  $\mathbf{d}_y^{k+1}$ , respectively. This plays a similar role to soft-thresholding for  $\ell_1$ , promoting sparse image gradients while better preserving large discontinuities such as edges.

### C. Dual Variable Updates

The scaled dual variables are updated to enforce consistency between  $\mathbf{u}$  and its gradient representations:

$$\begin{aligned} \mathbf{b}_x^{k+1} &= \mathbf{b}_x^k + (D_x \mathbf{u}^{k+1} - \mathbf{d}_x^{k+1}), \\ \mathbf{b}_y^{k+1} &= \mathbf{b}_y^k + (D_y \mathbf{u}^{k+1} - \mathbf{d}_y^{k+1}), \end{aligned} \quad (14)$$

where  $\mathbf{d}_x^{k+1}$  and  $\mathbf{d}_y^{k+1}$  are the outputs of the TL1 proximal operator in (13). These updates correspond to the ADMM dual ascent step, maintaining primal-dual consistency across iterations. We summarize the overall algorithm to minimize the TL1-regularized denoising model in Algorithm 1.

---

**Algorithm 1** TL1 Gradient Denoising via ADMM

---

**Require:** Noisy image  $\mathbf{f}$ , parameters  $a > 0$ ,  $\mu > 0$ ,  $\lambda > 0$ , maximum iterations  $K_{\max}$ , tolerance  $\varepsilon > 0$

**Ensure:** Denoised image  $\mathbf{u}$

- 1: Initialize  $\mathbf{u}^0 \leftarrow \mathbf{f}$ ,  $\mathbf{d}_x^0 \leftarrow \mathbf{0}$ ,  $\mathbf{d}_y^0 \leftarrow \mathbf{0}$ ,  $\mathbf{b}_x^0 \leftarrow \mathbf{0}$ ,  $\mathbf{b}_y^0 \leftarrow \mathbf{0}$
- 2: **for**  $k = 0$  **to**  $K_{\max} - 1$  **do**
- 3:    $\mathbf{u}^{\text{old}} \leftarrow \mathbf{u}^k$
- 4:   **u-update:** update  $\mathbf{u}^{k+1}$  via (11).
- 5:   **d-updates:**
- 6:      $\mathbf{z}_x^k \leftarrow D_x \mathbf{u}^{k+1} + \mathbf{b}_x^k$ ,  $\mathbf{z}_y^k \leftarrow D_y \mathbf{u}^{k+1} + \mathbf{b}_y^k$
- 7:      $\mathbf{d}_x^{k+1} \leftarrow \text{prox}_{\frac{1}{\lambda} \text{TL1}_a}(\mathbf{z}_x^k)$
- 8:      $\mathbf{d}_y^{k+1} \leftarrow \text{prox}_{\frac{1}{\lambda} \text{TL1}_a}(\mathbf{z}_y^k)$
- 9:   **dual updates:**
- 10:     $\mathbf{b}_x^{k+1} \leftarrow \mathbf{b}_x^k + (D_x \mathbf{u}^{k+1} - \mathbf{d}_x^{k+1})$
- 11:     $\mathbf{b}_y^{k+1} \leftarrow \mathbf{b}_y^k + (D_y \mathbf{u}^{k+1} - \mathbf{d}_y^{k+1})$
- 12:   **stopping: if**
- $\frac{\|\mathbf{u}^{k+1} - \mathbf{u}^{\text{old}}\|_2}{\max\{1, \|\mathbf{u}^{\text{old}}\|_2\}} < \varepsilon$ ,   **then break**
- 13: **end for**
- 14: **return**  $\mathbf{u}^{k+1}$

---

### III. NUMERICAL EXPERIMENTS

This section presents numerical experiments demonstrating the effectiveness of the proposed Algorithm 1. We compare the TL1-based method against several gradient-based regularization models:  $\ell_1$ -based total variation [1],  $\ell_1-\ell_2$  regularization [2], Minimax Concave Penalty (MCP) [3], and a combination of the logarithmic function and a high-order TV [9], referred to as LOG+TV. The codes of these competing methods were obtained from the respective authors.

Three benchmark images, “*Shapes*”, “*Peppers*”, and “*Cameraman*”, each of size  $512 \times 512$ , are used in the experiments, as shown in Figure 1. The *Shapes* image highlights geometric contours and piecewise-constant regions, which are suitable for evaluating edge preservation. The *Peppers* image contains smooth shading and subtle textures, challenging the algorithm to balance noise suppression and detail retention. The *Cameraman* image exhibits both structured edges and textured areas, providing a balanced test of noise removal and structure preservation.

All images are normalized so that their pixel intensities lie within the range to  $[0, 1]$ , before Gaussian white noise with standard deviation  $\sigma = 0.10$  is added. The quality of the denoised images is assessed using two widely adopted metrics: the peak signal-to-noise ratio (PSNR) and the structural similarity index (SSIM) [10]. Higher PSNR and SSIM values indicate better reconstruction fidelity and perceptual quality, respectively.

For each method, the regularization parameters were tuned via a Bayesian optimization method [11] implemented with MATLAB’s *BeyesOpt* function. All algorithms were terminated when the relative change between successive iterates was below  $10^{-4}$ , or after a maximum of  $K_{\max} = 200$  iterations.



Fig. 1: Clean benchmark images: (left) Shapes, (center) Peppers, and (right) Cameraman.

#### A. Qualitative Comparison

We first compare the visual quality of the denoised images. For the *Shapes* image, Fig. 2 illustrates that both MCP and TL1 produce visually appealing results. However, closer inspection of the geometric boundaries reveals that TL1 yields cleaner and more regular edges. In particular, along the upper edge of the bottom shape, the TL1 result almost completely removes the jagged artifacts that remain in the MCP and other competing methods, indicating improved edge preservation with reduced staircase effects.

For the *Peppers* image, Fig. 3 shows that all methods can suppress noise to some extent, but they differ significantly in their ability to retain fine details. The proposed TL1 model better preserves subtle structures around the pepper boundaries and highlight regions on the surface, where other methods either oversmooth the textures or leave residual noise. This suggests that TL1 achieves a favorable balance between noise removal and detail retention in natural images.

The *Cameraman* results in Fig. 4 and the zoomed patches in Fig. 5 further highlight the advantage of TL1. The proposed method maintains fine details such as the silos, camera tripod, and building edges, while still effectively suppressing background noise. In contrast, MCP tends to oversmooth the scene: the grass texture is largely wiped out and the silo is nearly blended into the background. The LOG+TV reconstruction also loses structural information in the building region and exhibits blurred textures. Overall, the qualitative comparisons demonstrate that TL1 consistently preserves edges and textures more faithfully than the other regularization models.

#### B. Quantitative Comparison

We next provide a quantitative comparison based on SSIM and PSNR for all methods and test images. Table I summarizes the denoising performance at noise level  $\sigma = 0.10$ . For the *Shapes* image, MCP attains the highest SSIM and PSNR, while TL1 achieves a competitive SSIM of 0.9300 with comparable PSNR, consistent with its visually clean and sharp edges. For the *Peppers* image, TL1 obtains the best SSIM (0.9054), indicating superior perceptual quality, whereas LOG+TV achieves the highest PSNR. For the *Cameraman* image, the proposed TL1 method clearly outperforms all competitors in terms of SSIM (0.8870), reflecting its ability to preserve fine structures and textures observed in Fig. 4 and Fig. 5. These results show that TL1 delivers consistently strong structural similarity across different image types, often achieving the best or near-best quantitative performance.

TABLE I: Quantitative comparison (SSIM / PSNR in dB) for all methods on three test images.

Method	Shapes		Peppers		Cameraman	
	SSIM	PSNR	SSIM	PSNR	SSIM	PSNR
$\ell_1$	0.9262	26.53	0.8725	28.32	0.8537	27.97
$\ell_1-\ell_2$	0.9278	26.57	0.8712	28.31	0.8539	27.97
MCP	0.9405	27.06	0.9042	28.21	0.8424	25.82
LOG+TV	0.8326	26.53	0.8555	29.18	0.8051	27.08
TL1 (Proposed)	0.9300	26.53	0.9054	28.33	0.8870	27.83

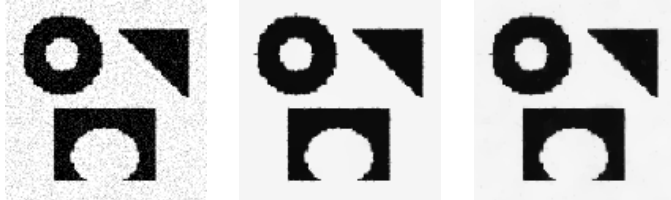


Fig. 2: Denoising results for Shapes. From left to right: Noisy, MCP, and TL1.



Fig. 3: Denoising results for Peppers. From left to right: Noisy, MCP, and TL1.

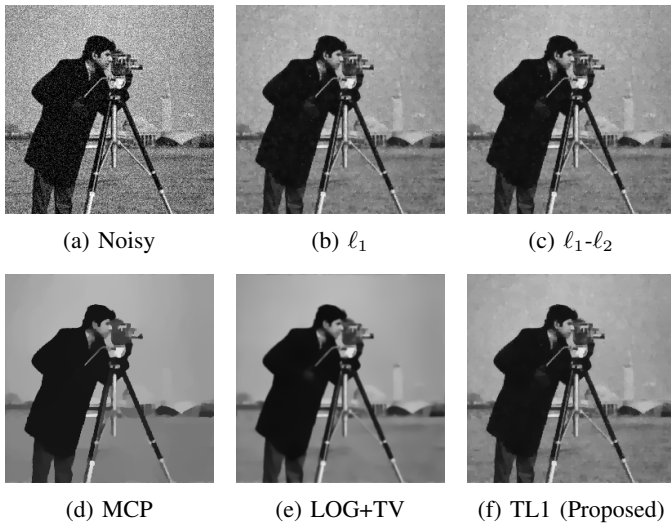


Fig. 4: Denoising results for Cameraman.

#### IV. CONCLUSION

We proposed an image denoising method based on TL1 gradient regularization solved via ADMM. The TL1 penalty provides a flexible nonconvex alternative to total variation, enhancing sparsity while better preserving edges and textures. Experiments on benchmark images show that the proposed ap-

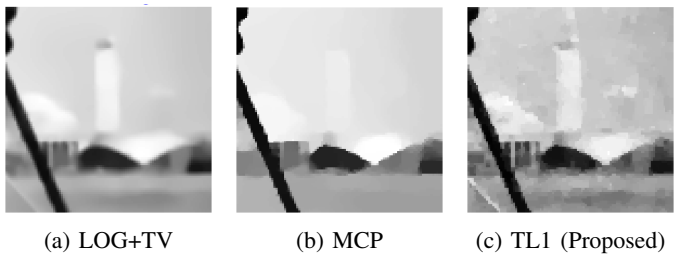


Fig. 5: Zoomed patches comparing texture and edge preservation. TL1 maintains fine details better than competing methods.

proach achieves higher structural similarity and visual quality than existing  $\ell_1$ - and nonconvex-based models. These results suggest that TL1 regularization offers a promising direction for robust and edge-preserving image restoration. Future work will extend this framework to other imaging inverse problems, such as deblurring, inpainting, and super-resolution, and explore adaptive parameter selection.

#### ACKNOWLEDGMENT

N. Choudhury was supported by the University of North Carolina at Chapel Hill Summer Undergraduate Research Fellowships (SURF) Program.

#### REFERENCES

- [1] L. I. Rudin, S. Osher, and E. Fatemi, “Nonlinear total variation based noise removal algorithms,” *Physica D: nonlinear phenomena*, vol. 60, no. 1-4, pp. 259–268, 1992.
- [2] Y. Lou, T. Zeng, S. Osher, and J. Xin, “A weighted difference of anisotropic and isotropic total variation model for image processing,” *SIAM Journal on Imaging Sciences*, vol. 8, no. 3, pp. 1798–1823, 2015.
- [3] J. You, Y. Jiao, X. Lu, and T. Zeng, “A nonconvex model with minimax concave penalty for image restoration,” *Journal of Scientific Computing*, vol. 78, pp. 1063–1086, 2018.
- [4] C. Wang, M. Tao, C.-N. Chuah, J. Nagy, and Y. Lou, “Minimizing  $1_1$  over  $1_2$  norms on the gradient,” *Inverse problems*, vol. 38, no. 6, p. 065011, 2022.
- [5] S. Zhang and J. Xin, “Minimization of transformed  $1_1$  penalty: theory, difference of convex function algorithm, and robust application in compressed sensing,” *Mathematical Programming*, vol. 169, no. 1, pp. 307–336, 2018.
- [6] S. Boyd, N. Parikh, E. Chu, B. Peleato, and J. Eckstein, “Distributed optimization and statistical learning via the alternating direction method of multipliers,” *Foundations and Trends in Machine Learning*, vol. 3, no. 1, pp. 1–122, 2011.
- [7] N. Parikh and S. Boyd, “Proximal algorithms,” *Foundations and Trends® in Optimization*, vol. 1, no. 3, pp. 127–239, 2014.
- [8] S. Zhang and J. Xin, “Minimization of transformed  $1_1$  penalty: Closed form representation and iterative thresholding algorithms,” *Communications in Mathematical Sciences*, vol. 15, pp. 511–537, 2017.
- [9] H. Fan, Q. Feng, R. Chen, X. Cao, and Z.-F. Pang, “A non-convex and non-smooth weighted image denoising model,” *Computers & Mathematics with Applications*, vol. 187, pp. 85–105, 2025.
- [10] Z. Wang, A. C. Bovik, H. R. Sheikh, and E. P. Simoncelli, “Image quality assessment: from error visibility to structural similarity,” *IEEE transactions on image processing*, vol. 13, no. 4, pp. 600–612, 2004.
- [11] J. Snoek, H. Larochelle, and R. P. Adams, “Practical bayesian optimization of machine learning algorithms,” in *Advances in Neural Information Processing Systems*, vol. 25, 2012, pp. 2951–2959.